Compton profile measurements with 662-keV γ rays

Maria Vittoria Heller and José Roberto Moreira
Department of Experimental Physics, Sao Paulo University, Sao Paulo, Brazil
(Received 30 July 1984; revised manuscript recieved 19 November 1984)

The Compton profile of Pb and Al was measured for three scattering angles (30°, 15°, 10°) using ^{137}Cs γ rays. A three-dimensional geometric correction was included by means of a Monte Carlo simulation to take into account finite-size effects of the γ source, target, and detector. Double scattering events were considered in the simulation and subtracted from the single profile when necessary. Good accordance with the theoretical momentum distribution of the electron cloud was observed when relativistic wave functions quoted by Biggs, Mendelsohn, and Mann were used. This accordance was achieved only when the Ribberfors correction was considered. The extension of the Compton profile to any scattering angle was verified experimentally.

I. INTRODUCTION

It is known that measurements of the Compton profile can provide information about the projection of the electronic momentum distribution on the scattering vector. The interpretation of experimental results requires the knowledge of the wave function of all the electrons of an atom so that knowledge of the Compton profile can serve as an excellent process to test wave functions obtained from different models.

Compton-profile measurements have become more frequent since 1970, when solid-state detectors of high resolution became available. Experimental results of Compton scattering for several elements are now available. However, most of the measurements were obtained for scattering angles near 180°, since the impulse approximation (see Ribberfors[1,2]) implies a differential cross section (in the nonrelativistic region) simply proportional to the Compton profile:

$$J(p_z)=\int\int dp_x dp_y\,\rho(\mathbf{p})\ .$$

Here, $\rho(\mathbf{p})$ is the momentum distribution of the electron system before scattering, and p_z is the component of the electron momentum, along the scattering vector. Ribberfors[1,2] showed that the conventional concept of the Compton profile also survives, even when high-energy γ rays force the consideration of relativistic effects. The author shows that the relationship between the differential cross section and the Compton profile valid for all scattering angles is

$$\frac{d^2\sigma}{dw'd\Omega'}=\frac{m^2r_0^2w'}{2w\,|\mathbf{k}-\mathbf{k}'|}\left[J(p_{\min})\frac{\tilde{X}}{E(p_{\min})}+\int_{p_{\min}}^{\infty}\frac{J(p)}{E(p)}\frac{d\tilde{X}_{\rm int}}{dp}dp\right], \quad (1)$$

where ω and ω' are the frequencies of the photon before and after scattering, $\mathbf{k}$ and $\mathbf{k}'$ the wave vectors of the incident and scattered photons, θ the angle of scattering, $d\Omega'$ the solid-angle element in the direction of $\mathbf{k}'$, and $\mathbf{p}$ and E the momentum and the total relativistic energy of the electron.

A good first approximation to $\rho_{\min}$ is

$$p_{\min}=\frac{m(\omega-\omega')-\omega\omega'(1-\cos\theta)}{|\mathbf{k}-\mathbf{k}'|}=p_z\ ,$$

$$\tilde{X}=\frac{R}{R'}+\frac{R'}{R}+2m^2\left[\frac{1}{R}-\frac{1}{R'}\right]+m^4\left[\frac{1}{R}-\frac{1}{R'}\right]^2\ ,$$

$$R\equiv\omega\left[E(p_{\min})-\frac{\omega-\omega'\cos\theta}{|\mathbf{k}-\mathbf{k}'|}p_z\right]\ , \quad (2)$$

$$R'\equiv R-\omega\omega'(1-\cos\theta)\ ,$$

$$\frac{d\tilde{X}_{\rm int}}{dp}=p\left[\frac{\omega'\sin\theta}{|\mathbf{k}-\mathbf{k}'|}\right]^2\left[F\left[\frac{1}{T^3}-\frac{1}{S^3}\right]+\frac{3m^4}{\omega^2}\left[\frac{m-D}{S^5}+\frac{m-D-W}{T^5}\right]\right],$$

where

$$D\equiv\frac{\omega-\omega'\cos\theta}{|\mathbf{k}-\mathbf{k}'|}p_z\ ,$$

$$H\equiv\left[\frac{\omega'\sin\theta}{|\mathbf{k}-\mathbf{k}'|}\right](p^2-p_{\min}^2)^{1/2}\ ,$$

$$S\equiv[(m-D)^2-H^2]^{1/2},\quad W=\omega'(1-\cos\theta)\ ,$$

$$T\equiv[(m-D-W)^2-H^2]^{1/2},\quad F=W-\frac{2m^2}{\omega}-\frac{2m^4}{\omega^2W}\ .$$

Considering that the second term of Eq. (1) is of the order p_z/m and can be neglected, Ribberfors[1,2] obtained

$$J_0(p_{\min})=\frac{2\omega\,|\,\mathbf{k}-\mathbf{k}'\,|\,E(p_{\min})}{mr_0^2\omega'\tilde{X}}\frac{d^2\sigma}{d\omega' d\Omega'}\ . \tag{3}$$

For experiments at 180° we would obtain

$$J_{180}(p_z)=\frac{2\omega[\,|\,\mathbf{k}-\mathbf{k}'\,|\,+p_z(\omega-\omega')/m\,]E}{m^2r_0^2X_{180}}\frac{d^2\sigma}{d\omega' d\Omega'}\ . \tag{4a}$$

This means that it is possible to calculate the Compton profile at any scattering angle θ $[J_0(p_{\min})]$ from the knowledge of $J_{180°}(p_z)$, providing we multiply the value calculated at 180° by the factor $f(p_z)$ obtained from Eqs. (3) and (4a), defined by Ribberfors[1,2] as

$$f(p_z)=\frac{X_{180}}{\tilde{X}[1+p_z(\omega-\omega')/m\,|\,\mathbf{k}-\mathbf{k}'\,|\,]} \tag{4b}$$

with the convenient renormalization.

We decided to make measurements at scattering angles different from 180° in order to verify the Ribberfors[1,2] considerations. Obviously this is based on the principle that there are "good" wave functions to describe atomic electrons. In this work we assumed that relativistic Hartree-Fock wave functions developed by Mendelsohn, Biggs, and Mann[3] were sufficiently accurate.

There are essentially two advantages in measuring the Compton profile at scattering angles differing from 180°. One of them is just experimental and is connected with the intensity of Compton scattering, because the cross section is large at small angles. For $\alpha\cong 1$ $(\alpha=\omega/m_0c^2)$, $d\sigma/d\Omega\cong 5\times10^{-26}$/electron for 30°, and $\cong 2\times10^{-26}$ cm^2/electron for 170°; see Evans.[4] The other is connected with an easier interpretation of data, because the occurrence of double and triple scattering can distort data remarkably (Cooper *et al.*[5]). *The spectral* distributions of double and triple scattering become narrow with an increase in scattering angle. This is expected since for a total scattering angle θ, the range of angles through which a photon may be deflected twice extends from θ to $(360°-\theta)$. So when we work at angles near 180°, the single-scattering γ ray has an energy very similar to the γ rays scattered twice. This increases the difficulty of separating single scattering from multiple scattering events. In the case of small scattering angles, the gammas from multiple scattering will be spread over a larger region of energy and this will affect the single Compton profile much less.

II. EXPERIMENTAL TECHNIQUES AND DATA PROCESSING

The experimental setup is shown schematically in Fig. 1. Photons of 662 keV from source F (^{137}Cs$\cong$30 Ci) are collimated by a 15-cm-long and 0.4-cm-diam cylinder and are incident on a sample located on a rotating platform.

The momentum distribution of orbital electrons measured in a Compton scattering experiment depends on the broadening of the scattered gamma-ray energy spectrum and also on the detector energy resolution. The momentum resolution improves with increasing γ-ray energy.[5]

The source selected has an intensity which permits the acquisition of data in time intervals of some hours. The disadvantage of this source is linked to the problem of shielding. This was solved by constructing a lead shield around and above the commercial container of the source, in such a way that the number of counts when the source was in its own case was the same when exposed inside our shielding.

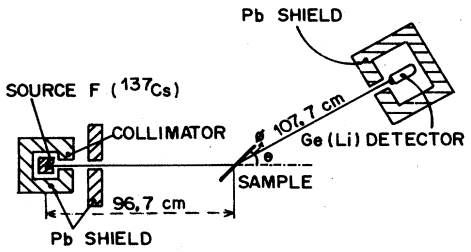

FIG. 1. Schematic diagram of the experimental system.

To align the center of the source, the collimator and the center of the sample, as well as to position the angle of the scattering, we used a He-Ne Laser. The sample was supported in a thin aluminum frame to minimize the effect of elastic and inelastic events from the support. The geometrical form of the sample was a parallelepiped with the dimensions shown in Table I.

The scattering radiation was counted by a Ge-Li Ortec detector of 40.3 mm diameter and 22.8 mm length, with an active volume of 26.8 cm^3. The total resolution given by the manufacturer was 2.3 keV at full width at half maximum (FWHM) for 1.33-meV photons. This detector was placed on a moving platform that could support a weight of $\cong$600 Kg of shielding; attached to this platform there was a thick iron rod connected with the base of the scatterer table. The Ge-Li detector was assembled inside a shield of lead and preceded by a collimator 1.2 cm in radius and 10 cm thick. This structure allows detector positioning at several scattering angles in relation to the sample.

The energy calibration was done with calibrated sources of ^{154}Eu and ^{22}Na for every scattering angle; typical channel width is 0.3 keV/channel. The relative detector efficiency was measured with ^{154}Eu γ rays in the region of interest (510 to 660 keV). Figure 2 shows that the efficiency variation (13%) of the detector can be described with reasonable precision by a straight line in this range.

The scattering angles selected for the experiment were 30.1°$\pm$0.7, 15.0°$\pm$0.4, and 10.9°$\pm$0.3. Systematic measurements of the two elements (Pb, Al) over reasonable time spans (some hours) were performed. A typical spectrum is shown in Fig. 3.

TABLE I. Dimensions of the samples.

Element	Width (mm)	Length (mm)	Thickness (mm)
Pb	20.0	50.0	2.0
Al	19.8	60.3	19.6

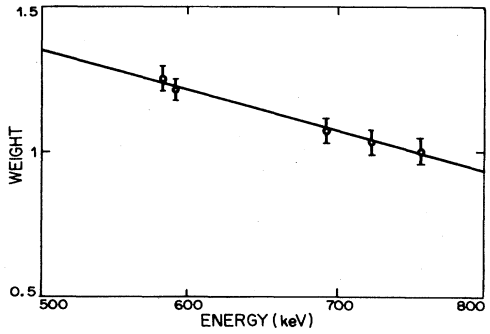

FIG. 2. Efficiency of the detector in the region of interest.

The spectra were corrected by subtracting the background and taking into account the detector's efficiency; then they were fitted to a function that is the addition of a Laurentzian and a Gaussian function plus a straight line:

$$y=A_1+A_2(x-A_4)+\frac{A_3(A_5x)^2}{(x^2-A_4^2)^2+(A_5x)^2}+A_6e^{-(x-A_7)^2/2A_8^2}. \quad (5)$$

In Table II we present the best-fit results of the experimental data for the two elements; for one of the elements we have spectra for two different sample thicknesses (the sample thickness is listed in Table I and double thickness is twice the single sample thickness). The figures quoted under the χ^2 column are the χ^2 per degree of freedom.

We note that in cases of single and double thickness ($\epsilon_{1/2}$) the FWHM did not show remarkable variations that could be attributed to double scattering. However, at low energy far from the Compton peak, the counting rate, although small (factor of $\frac{1}{100}$ in relation to peak) was not zero due to double scattering.

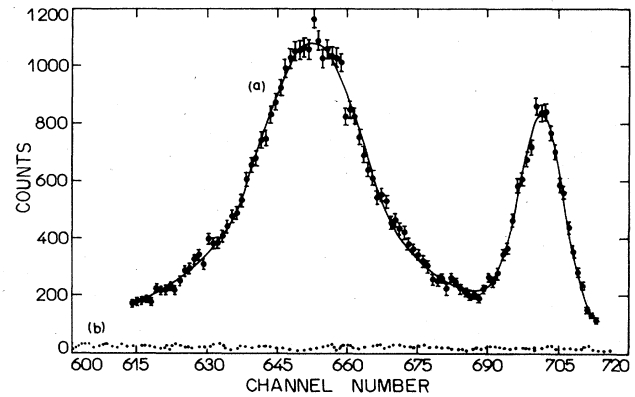

FIG. 3. Spectrum of Compton scattering with ^{137}Cs γ rays, sample Pb, $\theta=10°$. (a) Spectrum of Compton scattering; (b) background.

III. SIMULATION OF CROSS SECTION

To make a comparison of our experimental results with theoretical predictions, we constructed the spectral distribution of scattered gammas using electronic wave functions. The procedure may be summarized as follows.

(a) Discrete values of the single scattering Compton profile were taken from the work of Mendelsohn, Biggs, and Mann[3] (relativistic Hartree-Fock functions).

(b) Continuous functions were adjusted from the values of single Compton profile for each orbital, in order to obtain $J_{180}(p_z)$, Eq. (4a), for every p_z value.

(c) Since these single Compton profiles are calculated for angles of 180°, we made the correction described in Eq. (4b) for the scattering angle studied, yielding $J_0(p_{\min})$ from Eq. (3).

(d) Differential cross sections were then calculated [$d^2\sigma/d\omega' d\Omega'$ from Eq. (3)], using the computational Monte Carlo method to simulate the theoretical γ-ray spectra, characterized by ω' and θ. When performing the calculation the instrumental γ-ray broadening was inserted using the expression

$$\omega'=\omega'+Y_1\Gamma_{\text{resol}}, \quad (6)$$

where

$$Y_1=\sqrt{-2\ln r}\sin(2\pi r),$$

r is a random number, and Γ_{resol} is the resolution of the elastically scattered γ ray.

Although we followed the suggestion of Felsteiner,[6–8] item (d) deserves some additional remarks.

(1) From that author we see that the γ beam is assumed to arrive at right angles with the base of the specimen. In our case we calculated the path of the incident γ by assuming it propagates in a cone defined by the collimator. Due the small collimator apperture, the random selection of the departure direction was made as suggested by Williams[9] to accelerate the computational simulation.

(2) In the Monte Carlo procedure the atomic shell of the scatterer electron is selected at random, taking into account the number of electrons in each shell (see Felsteiner[6–8]).

(3) For the evaluation of double scattering the computation is longer, because the cross section depends on the γ polarization. In the place of the $\tilde{X}$ factor defined in Eq. (2) we must use the expression given by Ribberfors[1,2] for polarization along the x and y axes. This is important only for the second scattering as the incident beam is considered unpolarized. After leaving the sample, the polarization is no longer important because the detector is not sensitive to this γ ray state.

(4) Departure cone. Considering the small solid angle subtended by the detector at the scatterer it was necessary to adopt a technique similar to that mentioned in item (1) to accelerate the theoretical simulation. When leaving the scatterer the gamma had its direction chosen at random in a cone subtended by an area twice the area of the detector, concentric with it. Into this solid angle ($\cong 2\times10^{-3}$ sr) we assumed a constant cross section and gave to the scattered γ a weight obtained from the ratio of the differential cross section $d\sigma/d\Omega$ and the integral cross section.

TABLE II. Comparison of experimental and theoretical results for the three scattering angles (30.1°, 15.0°, and 10.9°) for the two elements studied.

Angle	Element	Thickness	$\epsilon_{1/2}$ (keV) experimental	χ^2	$\epsilon_{1/2}$ (keV) theoretical	χ^2
30.1°	Pb	single	14.21±0.95	0.952	15.00±1.04	1.240
		double	14.16±0.89	1.130		
	Al	single	10.53±0.63	1.470	10.87±0.75	1.960
15°	Pb	single	8.58±0.51	1.002	9.24±0.64	1.480
		double	9.24±0.55	1.423		
	Al	single	6.40±0.38	0.978	7.06±0.49	1.01
10.9°	Pb	single	9.00±0.54	1.110	8.10±0.56	1.180
		double	8.00±0.48	1.19		
	Al	single	6.54±0.39	1.346	6.53±0.45	0.824

IV. ANALYSIS OF RESULTS

From the computational simulation it was possible to construct the energy spectrum of the scattered gamma rays. In Fig. 4 we see a Compton spectra for Al at 30°, considering the geometry of the experiment for a realistic situation (orbital electron in movement) and in an ideal situation of electrons at rest. We see clearly the contribution imposed by the two wave functions. Table III gives the FWHM of the simulated spectra for the two elements calculated at $\theta=30°$. This enlargement in the spectra caused by the electron's movement decreases with the scattering angle, but it is still adequate to give information on the electronic momentum distribution at angles larger than 10°.

To reproduce the experimental spectra from calculation we must consider the double-scattering contribution. The histograms of Fig. 5 show the double-scattering contribution in relation to single scattering for Pb. The total number of double events in the region of interest is 2%, and its spectrum is reasonably approximated by a straight line associated with the straight line used for the correction for detector efficiency. For Al, double events are only 1% of the single.

The precision of our computational simulation of double scattering was tested by reproducing the results of Cooper *et al.*[5] for 412 keV and 167.9°, where we obtained 16.4% for the double Compton contribution against the cited values of $\cong$20%. Figures 6–9 show some of the experimental results obtained with background substration and correction for detector efficiency. We also display the spectra obtained by computational simulation.

Table II shows the theoretical and experimental data, with the values of ($\epsilon_{1/2}$) obtained from the fitting of the analytic functions (Gaussian plus Laurentzian function) to the Compton measured spectra, and also to the points obtained from the histograms of the computational simulation. The value of $\epsilon_{1/2}$ is obtained measuring the FWHM.

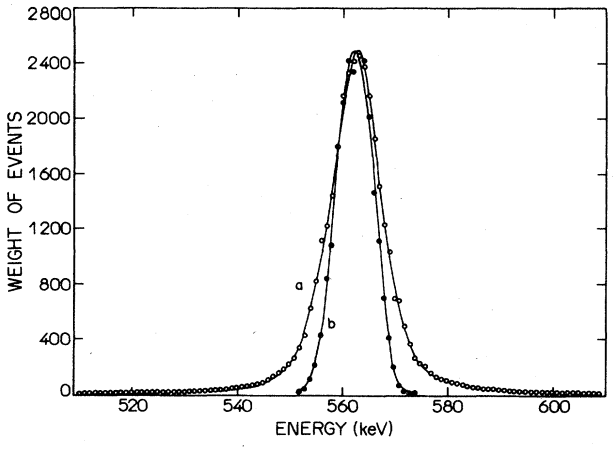

FIG. 4. γ-ray energy distribution for Al, at $\theta=30°$; curve *a*, for $p_z\neq0$; curve *b*, for $p_z=0$.

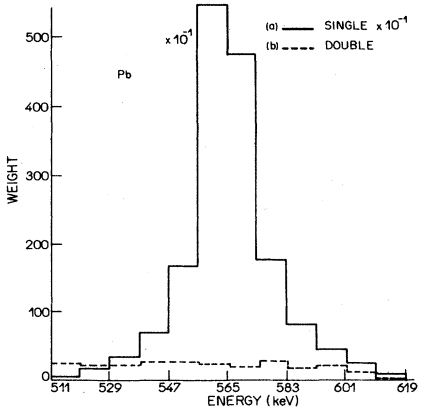

FIG. 5. Single and double Compton profile for Pb, $\omega=662$ keV, $\theta=30°$, specimen of 0.2 cm thickness.

TABLE III. FWHM of the energy distributions for the two elements at $\theta=30°$, under the same geometry, for $p_z\neq 0$ and $p_z=0$. p_z is the component of the electron momentum, along the scattering vector.

Element	$\epsilon_{1/2}$ (keV)	$\epsilon_{1/2}$ (keV)
Pb	15.00±1.00	8.44±0.56
Al	10.87±0.75	8.52±0.57

Some values of χ^2 are unsatisfactory, as in the case of Al at 30° ($\chi^2=1.960$); however, as the fitting for other angles is good, we cannot conclude that any systematic error associated with the Al wave function exists. For 10° and 15°, there is practically no contribution of the K shell for Pb, in agreement with energy conservation. This advantage, that in principle would permit the improved observation of the profile of the more external electron shells, was useless from a practical point of view since the contribution of these two electrons when compared with the others is not significant in our experimental results, in accordance with the computational simulations. This can be explained because the region of high energy of the Compton spectrum can be examined only up to 655 keV due the presence of the elastic peak that hides it. In the spectrum at 15° (10°) the center of the Compton peak is at 634 (649,3) keV, which allows the examination of a total-energy variation of 21 (6) keV. At 21 (6) keV we were working with maximal values of p_z equal to 6 (1.6) a.u. For this p_z value the contribution of the K shell in the total Compton profile (Biggs[3]) for Pb is 0.5% (1.5%). The investigation of the low-energy side of the Compton profile is also limited, by energy considerations, at 574 keV. Therefore, for 15° (10°) we can investigate the absence of

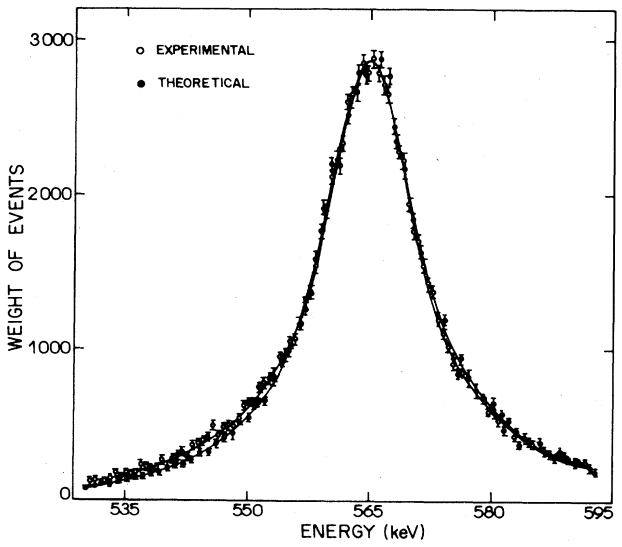

FIG. 6. γ-ray energy distribution for Pb at 30°, experimental and theoretical results.

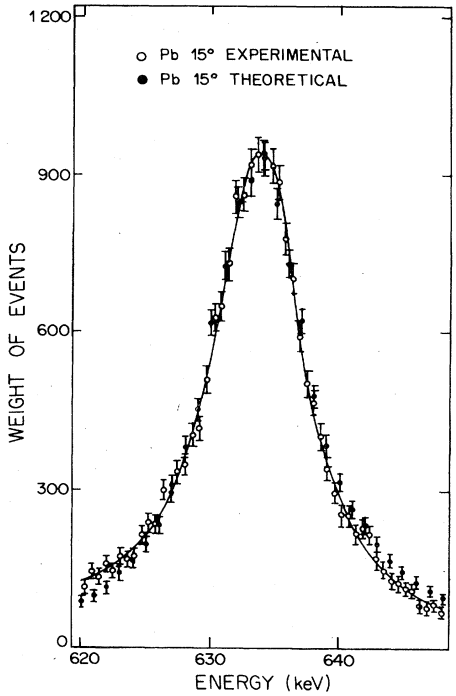

FIG. 7. γ-ray energy distribution for Pb at 15°, experimental and theoretical results.

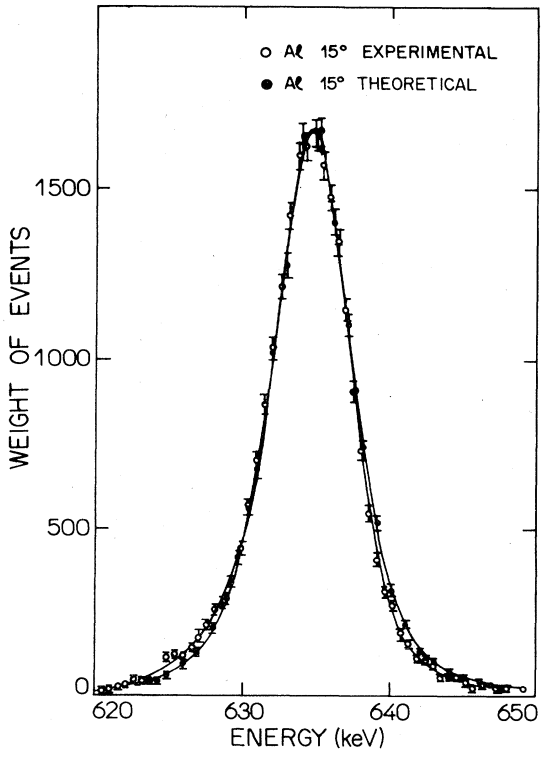

FIG. 8. γ-ray energy distribution of Al at 15°, experimental and theoretical results.

TABLE IV. Comparison of the Compton profile obtained with and without Ribberfors's correction for Pb. Energy of the incident photon is 662 keV.

Angle	Element	$\epsilon_{1/2}$ (B)[a]	$\epsilon_{1/2}$ (R)[b]	$\epsilon_{1/2}$ (exp)[c]
30°	Pb	13.27±0.50	15.00±1.04	14.21±0.95
169°	Pb	10.55±0.62	10.51±0.63	

[a] $\epsilon_{1/2}$ (B) is FWHM distribution obtained without Ribberfors's correction.
[b] $\epsilon_{1/2}$ (R) is FWHM distribution with Ribberfors's correction.
[c] $\epsilon_{1/2}$ (exp) is the FWHM of the experimental distribution.

the K-shell contributions up to 60 (75) keV, below the Compton peak corresponding to a p_z of 16 (20) a.u. In this p_z region the contribution of the K shell is 2 (3)%. As this K-shell participation is low, it is difficult to detect. It shows up only as a discontinuity in the spectra tail, at an energy of about 574 keV, where the number of measured events is much less than in the peak [$\cong$4 (3%)]. Fluctuations of this order (2 or 3% over 4 or 3%) mean a discontinuity of only 0.1% of the peak value. Total counts at the peak of our typical spectra are near 2500 counts, which leads to a fluctuation of 3 counts for this effect.

In Pb (10°) the computer simulation of the high-energy region presents differences of 1.5%, between inclusion and not inclusion of the K shell. In our experimental spectrum (Fig. 9) there are an average of 600 counts/channel (uppermost visible part of the tail) with a statistical error of 4%. Considering the occurrence of $\cong$10 experimental points in the region, we are close to being able to distinguish between the fits with and without the K shell. Unfortunately, the χ^2 variation in the fit does not allow us to draw a conclusion. An examination of the low-energy region is even less appropriate for detecting this effect. Results obtained with other elements (W, Ag, and Cu) will be published.

Our results, based on the scattering of a metallic target, could be criticized for the uncertainty of the wave function of the more external electrons. Tests of sensibility of the contribution to Compton spectra of these electrons were done through computational simulation. Figure 10 compares Compton simulated spectra for Pb with and without shells $6s$, $6p$ (4 electrons). In this extreme situation (4 electrons removed) we observed a small difference that manifests itself in values of $\epsilon_{1/2}$, 14.81±0.59 keV as compared with the all shells result of 13.27±0.50 keV.[10] Uncertainties associated with the $\epsilon_{1/2}$ value are evaluated through spectrum simulation (spectra with 80000 events, compatible with the total number of experimental events) using different random numbers at the start of the computation, with an histogram channel width of 0.3 keV, compatible with our experimental resolution. In a real situation, in which approximately a single electron leaves the shell, the differences between the $\epsilon_{1/2}$ values must decrease. Supposing half the difference of the values es-

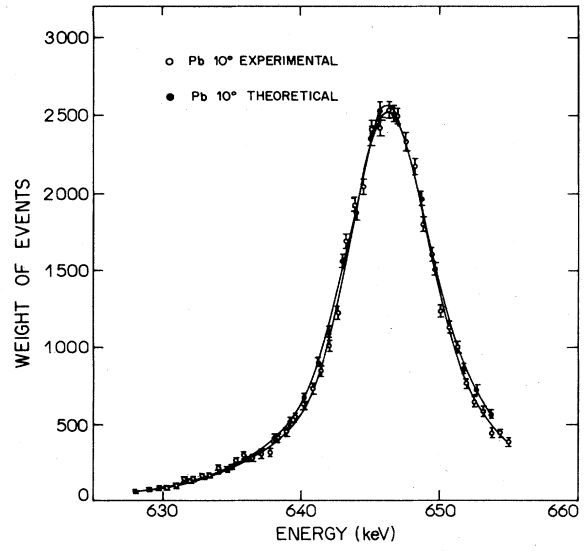

FIG. 9. γ-ray energy distribution for Pb at 10°, experimental and theoretical results.

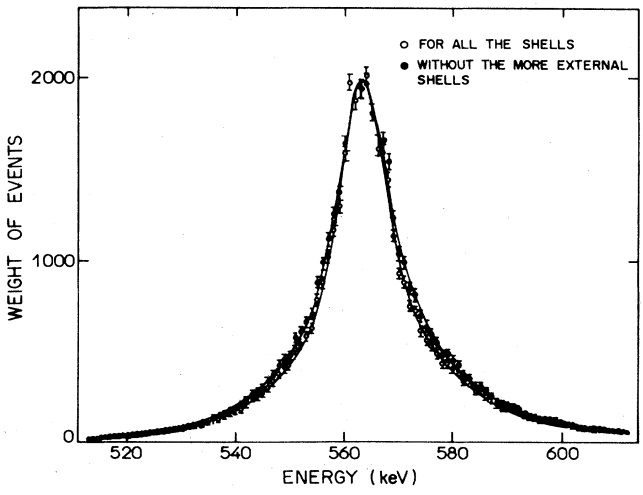

FIG. 10. γ-ray energy distribution for Pb, at 30°, (a) for all the shells and (b) without the more external shells $6s$, $6p$.

timated in the simulation $(14.81-13.27)/2=0.75$ we observe that there is a possibility of detecting this effect if the uncertainty in $\epsilon_{1/2}$ is reduced to about 0.3 keV. This uncertainty requires a spectrum with a higher number of events ($\cong 300\,000$ counts). For our experimental situation spectrum acquisition would be longer than 50 h, requiring a stability better than 0.15 keV in 600 keV. This kind of stability for the electronic system is at the limit of what can be obtained today. The situation for lighter elements is more favorable.

V. CONCLUSION

Our work shows that it is possible to reproduce the experimental results through a computational simulation using the Ribberfors[1,2] expressions for angles differing from 180°. The noninclusion of this correction gives rise to a systematic discrepancy discernible in all spectra.

Table IV shows the differences with and without Ribberfor's correction for a scattering angle of 30°, and for an angle of 169°.

Recent work of Halonen[11] comments that there was only a small difference in the evaluation of double Compton scattering when Ribberfors's correction is used. This effect, however, is important in the cases of simple scattering. Following Ribberfors's[1,2] suggestion, experiments of Compton scattering with polarized photons could better distinguish the differences between the Klein-Nishina and the Ribberfors cross sections. For the special case of heavy elements it would be possible with our experimental arrangement, but with much longer time, to detect the contribution of the K shell.

ACKNOWLEDGMENTS

We are deeply indebted to Professor Max Cohenca and Professor Philippe Gouffon of the Physics Institute of the University of Sao Paulo for helpful collaboration in all aspects of the computations. The authors are grateful to Professor Wayne Seale for useful comments on the manuscript.

[1]R. Ribberfors, Phys. Rev. B **12**, 2076 (1975).
[2]R. Ribberfors, Phys. Rev. B **12**, 3136 (1975).
[3]L. B. Mendelsohn, F. Biggs, and J. B. Mann, At. Data Nucl. Data Tables **16**, 202 (1975).
[4]R. D. Evans, *The Atomic Nucleus* (McGraw-Hill, New York, 1955).
[5]M. Cooper, P. Pattison, and J. R. Schneider, Philos. Mag. **34**, 243 (1976).
[6]J. Felsteiner, P. Pattison, and M. Cooper, Philos. Mag. **30**, 537 (1975).
[7]J. Felsteiner and P. Pattison, Nucl. Instrum. Methods **124**, 449 (1975).
[8]J. Felsteiner and P. Pattison, Phys. Rev. B **13**, 2702 (1976).
[9]I. R. Williams, Nucl. Instrum. Methods **44**, 160 (1966).
[10]These results were obtained with a simulation using values for the collimator and detector radii slightly inferior to the experiment.
[11]V. Halonen and B. Williams, Phys. Rev. B **19**, 1990 (1979).